DOI: 10.13009/EUCASS2019-353

DOI: ADD DOINUMBER HERE

Simulations of turbulent combustion and wall heat transfer in single and multi injectors GCH4/GOx rocket combustors

G. Indelicato[*], *P. E. Lapenna*[†], *D. Durigon*[‡], *F. Creta* [§]
Sapienza, University of Rome
via Eudossiana 18, 00184, Rome, Italy
giuseppe.indelicato@uniroma1.it

Abstract

In the present work a methodology is proposed for the modelization of wall heat fluxes within operative rocket combustion chamber conditions. It is based on a newly developed non-adiabatic flamelet model that can be used to both wall resolved simulations as well as with wall functions for the boundary layer resolution. In the latter a calibration technique for the turbulent Prandtl number at wall is proposed, based on the results obtained on the wall resolved simulations. The proposed strategy is then applied to 2D and 3D simulations of experimental single and multi-element gaseous-methane/gaseous-oxygen (GCH4/GOX) rocket combustors and tested against experimental reseults in terms of wall heat flux and pressure drop on the chamber wall. Two flamelet tabulation techinques are also investigated: the non-adiabatic model and the semi-adiabatic one. The comparison is carried both on the generated flame structures and on the simulation results tested against experiments.

1. Introduction

In spite of the efforts and the achievements in the design of advanced and reusable liquid rocket engines (LRE) in the last years, the correct wall heat flux prediction within the thrust chamber and the consequent design of the cooling system still represent a crucial aspect. Rocket chambers generally experience extreme thermal environments, with temperatures exceeding 3500 K. Furthermore, the trend of increasing chamber pressures, optimizing performances and reducing weights, causes the wall heat flux to increase almost linearly, requiring trade off design solutions.

In this context the numerical simulation of reacting flows inside a combustor is a useful tool whose reliability has been largely proved.[13,21] Nonetheless the incorporation of non-adiabatic effects, particularly dominant as the flame approches the chamber wall, is an on-going research field which has attracted different authors in the recent years.[6,11,15,18,22,23] Different approaches have been used to model the combustion process; a common assumption for the simulation of H_2/O_2 fueled rocket engines is that of chemical equilibrium, owing to the typical fast timescales involving hydrogen oxidation.[11] In the case of hydrocarbon combustion, however, several species are involved requiring a more detailed chemistry modelization. In this context the classical flamelet theory[16] developed by Peters showed good performances in capturing detailed kinetics effects by means of a decomposition between the mixing and the flame structure problem, under the assumption of high *Da* numbers. The latter in particular is solution of a 1D problem under the imposition of a thermodynamic pressure p_0 and allows the tabulation of all the thermo-chemical properties of the mixture in the flamelet libraries which can be referred to as thermodynamic manifolds, for which a generic thermodynamic variable ψ can be expressed as

$$\psi = \psi(Z, \chi_{st}) \tag{1}$$

being χ_{st} the scalar dissipation rate of the mixture fraction Z at the stoichiometric value. An extension of this model to include non-adiabatic effects was originally proposed by Lentini and Marracino[12] to model radiation in non-luminous diffusive flames, with the introduction of an enthalpy defect ϕ defined as the difference between an enthalpy ensuing

[*]Ph.D Student, Department of Mechanical and Aerospace Engineering. E-mail: giuseppe.indelicato@uniroma1.it
[†]Research Fellow, Department of Mechanical and Aerospace Engineering. E-mail: pasquale.lapenna@uniroma1.it
[‡]Engineer at Interconsulting s.r.l . E-mail: durigon.diego@gmail.com
[§]Associate Professor, Department of Mechanical and Aerospace Engineering. E-mail: francesco.creta@uniroma1.it

DOI: 10.13009/EUCASS2019-353

from the adiabatic and steady state solution of the flamelet equations[16] and the actual non-adiabatic enthalpy of the flow,

$$\phi = h - h_{ad}(Z) = h - [h_O + Z(h_F - h_O)]. \tag{2}$$

being h_O and h_F respectively the enthalpy of the oxidizer ($Z = 0$) and of the fuel ($Z = 1$) streams. In spite of the good results obtained extending this model to rocket engines applications,[7,10] some limitations were noticed in the presence of high heat loss such as those present in LRE combustion chambers, which required the imposition of a cut-off temperature to avoid unphysical values.

In the present work a predictive methodology is proposed for the evaluation of wall heat flux within operative rocket combustion chamber conditions. On the basis of low-Mach number assumptions,[8,9] an unsteady Reynolds averaged Navier Stokes (uRANS) framework in conjunction with a flamelet-based method for turbulent combustion modeling,[17] it relies on the introduction of a newly developed non-adiabatic flamelet model. The latter is based on the standard defect method,[12] with the introduction of a functional dependence modulating the enthalpy loss in the mixture fraction space, following the work of Kim et al.[6] The main feature of the new model is to localize the maximum of the enthalpy loss to the mixture fraction corresponding to stoichiometric mixing conditions.The proposed strategy is assessed involving different flamelet models, from the frozen to the newly developed one. The theoretical formulation and the description of the new model is given in the following section. The proposed methodology is then applied to 2D and 3D simulations of a GOx/GCH4 single-injector combustor[14] and a seven element multi-injector chamber.[19] Both the combustors were developed at the Chair of Turbomachinery and Flight Propulsion of the TUM. Results are compared with experiments providing model validation.

2. Theoretical and numerical formulation

2.1 Non-adiabatic flamelets

The proposed non-adiabatic flamelet model relies on the standard defect method,[12] with the introduction of a functional dependence modulating the enthalpy loss in the mixture fraction space. The main conjecture is to localize the maximum energy loss at the mixture fraction point corresponding to the stoichiometric value, Z_{st}, assuming there the maximum temperature and so the majority of heat exchange. Non-adiabatic flamelets are therefore computed by solving for species mass fractions Y_i and imposing, for each user-prescribed ϕ, a steady state enthalpy profile $h(Z)$

$$\partial_t Y_i - \frac{\chi}{2}\frac{\partial^2 Y_i}{\partial Z^2} = \frac{\omega_i}{\rho} \tag{3}$$

$$h(Z) = h_{ad}(Z) - \phi \cdot f(Z, Z_{st}) \tag{4}$$

being χ the scalar dissipation rate of the mixture fraction, ω_i the source term of ith-species and ρ the density of the mixture. The function modulating the defect, albeit reasonable, is arbitrary and should be validated by means of a paradigmatic DNS study of a diffusive flame impinging on a non adiabatic wall, revealing the distribution of enthalpy across the mixture fraction space, which is however not currently available. In eq. (4) the parameter ϕ represents the maximum enthalpy loss localized at Z_{st}. Conversely, $f(Z, Z_{st})$ is the normalized function modulating the defect. It is assumed piece-wise linear

$$f(Z, Z_{st}) = \begin{cases} \frac{Z}{Z_{st}} & Z \leq Z_{st} \\ 1 - \frac{Z - Z_{st}}{1 - Z_{st}} & Z > Z_{st} \end{cases} \tag{5}$$

and is parameterized in Z_{st} in such a way that $f(Z = Z_{st}) = 1$. An example of flamelet structures generated by solving eqs. (3-4) using the detailed chemical mechanism GRI 3.0[20] for an oxygen-methane mixture ($p = 20$ bar, $T_{ox} = 278$ K, $T_f = 269$ K, $Z_{st} = 0.2$) is given in Figs. 1-2. The present conditions refer to the experimental multi-injector chamber described in.[19] Particularly interesting from Fig. 2 is the CO_2 profile, showing clearly how as the enthalpy level of the mixture is lowered, the endothermic dissociation reactions leading to the formation of CO are increasingly suppressed, thus leading to an increased content of CO_2 with respect to adiabatic conditions.

2.2 Semi-adiabatic flamelets

In the semi-adiabatic approach, mixture properties are subject to non adiabatic effects only in terms of temperature while the mixture composition is frozen and kept equal to the adiabatic one. This assumption translates in considering

DOI: 10.13009/EUCASS2019-353

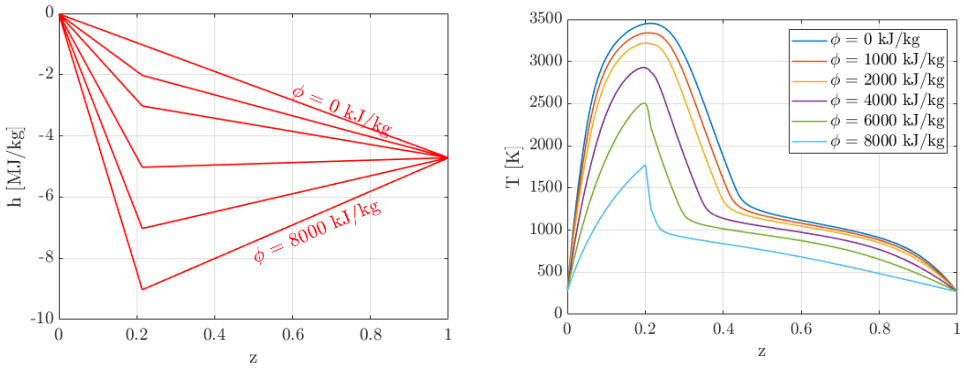

Figure 1: Enthalpy (left) and temperature (right) profiles at $\chi = 0\ s^{-1}$ for different defect values ϕ

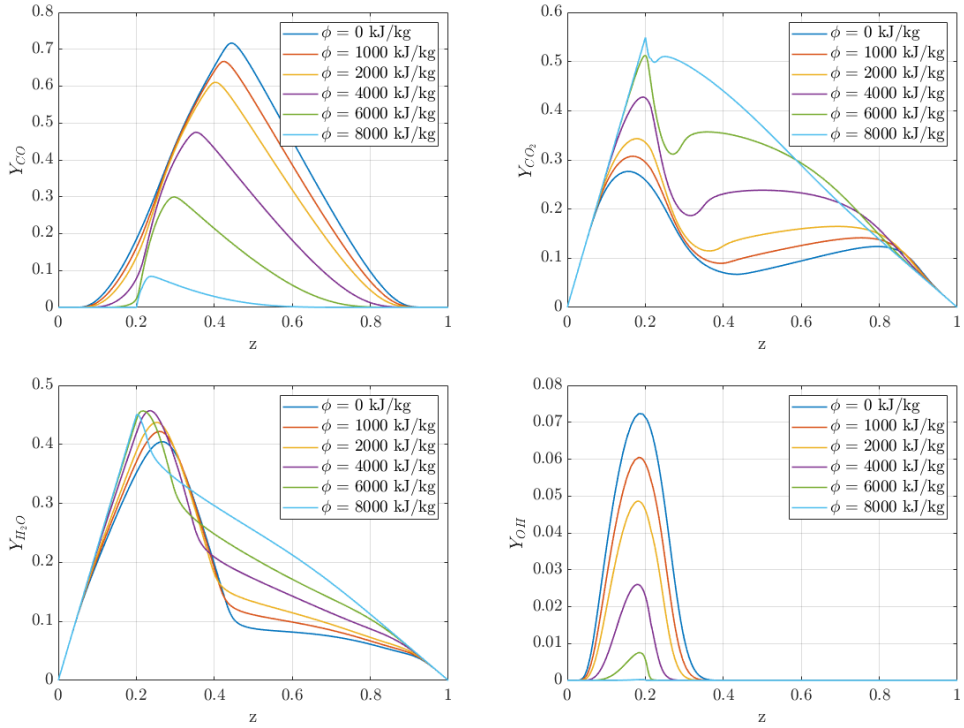

Figure 2: Mass fractions of the main combustion products and intermediate species at $\chi = 0\ s^{-1}$ for different defect values ϕ

only the composition profiles corresponding to $\phi = 0$ (see Fig. 2). We are therefore implicitly assuming reaction rates to vanish as temperature decreases, thus preventing further reactions, such as recombinations close to the wall. Practically, enthalpy loss causes temperature to decrease accordingly to the profile prescribed in eq. (4). The thermodynamic mixture properties are then evaluated according to this temperature but with the frozen composition. Therefore for a generic thermodynamic quantity ψ we have

$$\psi = \psi(p_0, T, Y^f) \tag{6}$$

where the superscript f denotes frozen composition, p_0 is the thermodynamic pressure at which the flamelets are calculated and T the non-adiabatic temperature. An overview of the semi-adiabatic flamelets and a comparison with the non-adiabatic ones is given in Fig. 3.

As clearly observable, for a fixed enthalpy defect we have a more pronounced temperature decrease for the frozen flamelets, which would even lead to unphysical temperatures if a cut-off at 269 K was not imposed. That means that a general non-adiabatic temperature is obtained for a lower defect in the frozen method than in the non-adiabatic case. This is also shown in Fig. 4, reporting the upper stable branch of the S-curve plotted for the two non-adiabatic models. The greater sensitivity to enthalpy losses can be explained by first considering that the frozen flamelets do not allow

DOI: 10.13009/EUCASS2019-353

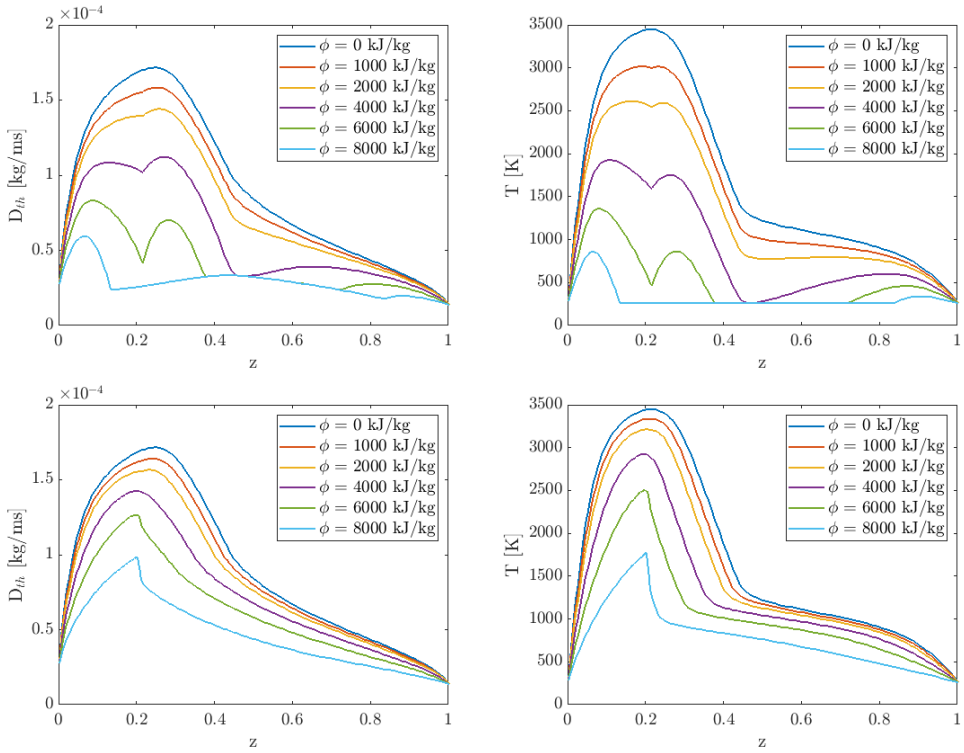

Figure 3: Equilibrium flamelets at different enthalpy defects obtained with the semi-adiabatic approach (top) and the non-adiabatich method (bottom). Plotted are the thermal diffusivity and the temperature of the mixture.

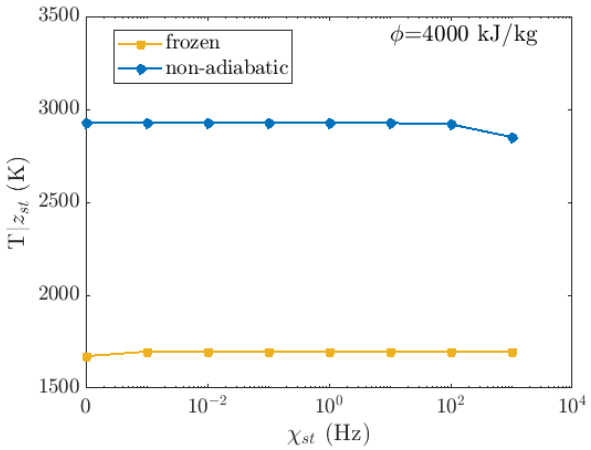

Figure 4: Upper branch of S-shaped curves for the two non-adiabatic models, frozen and non-adiabatic, and a given ϕ = 4000 kJ/kg. In abscissa stoichiometric scalar dissipatio values ranging from equilibrium (χ_{st} = 0 Hz) to 1000 Hz; in ordinata temperature conditioned to the stoichiometric mixture fraction value.

DOI: 10.13009/EUCASS2019-353

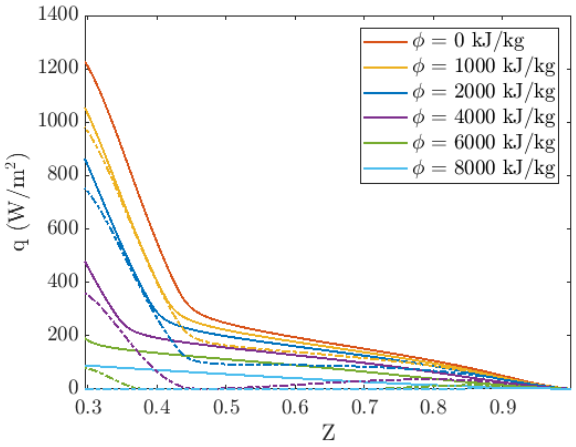

Figure 5: Predicted wall heat flux reconstructed from tabulated equilibrium values with a semi-adiabatic (dashed) and the new non-adiabatic (solid) model. A wall temperature value of 350 K is assumed.

for recombinations at wall and thus neglect a heat source that may sustain the flame even at low enthalpies; moreover the frozen approach leads to higher concentration of lighter species than the non-adiabatic ones, with a lower thermal inertia, easier to be cooled down. This also justifies a greater thermal diffusivity in the frozen flamelets, for a fixed temperature value. The importance of recombination at lower enthalpies is also showed using the approach employed by Perakis and Haidn in,[15] where a normalized wall heat flux using tabulated flamelet values for the frozen and the non-adiabatic case has been calculated, assuming a wall temperature of 500 K. This was done in order to give a prediction of the wall heat flux ensuing from a CFD analysis employing those flamelet libraries. The same analysis is carried in the following employing the two sets of flamelets previously described.
Fig. 5 suggests that differences in the wall heat flux are small as long as we are in the fuel reach region of the mixture fraction space. This is generally the situation we have in proximity of the injection plate, where the coaxial injected fuel forms a recirculation zone. In this region therefore, small differences between the methods are expected in the resulting wall heat flux. As we move towards the stoichiometric value, these differences become relevant even for relatively small defects, i.e $\phi = 2000$ kJ/kg.

3. URANS numerical framework

In the present work we use the unsteady URANS solver `RflameletSmoke`[7] developed in the context of the OpenFoam-based framework `OpenSMOKE++`.[2] It is based on a pressure-based number framework in conjunction with a flamelet-based method for turbulent combustion modeling. Flamelet-based methods allow a detailed chemical description of the flame structure at a reasonable computational cost and avoid the combustion induced stiffness of the numerical integration. Moreover, in the low-Mach number limit, flamelet based tabulation methods for turbulent non-premixed combustion are well-posed, and provide a properly filtered/averaged treatment of thermochemical properties.[8] The code solves transport equations for enthalpy $\widetilde{h}$, mixture fraction $\widetilde{Z}$ and its variance $\widetilde{Z''}$, in addition to mass and momentum equations

$$\partial_t(\bar{\rho}\cdot\widetilde{Z}) + \nabla\cdot(\bar{\rho}\widetilde{\mathbf{u}}\cdot\widetilde{Z}) = \nabla\cdot\left[\left(\bar{\alpha}+\frac{\bar{\rho}\nu_t}{S\,c_t}\right)\nabla\widetilde{Z}\right] \tag{7}$$

$$\partial_t(\bar{\rho}\cdot\widetilde{h}) + \nabla\cdot(\bar{\rho}\widetilde{\mathbf{u}}\cdot\widetilde{h}) = \nabla\cdot\left[\left(\bar{\alpha}+\frac{\bar{\rho}\nu_t}{Pr_t}\right)\nabla\widetilde{h}\right] \tag{8}$$

$$\partial_t(\bar{\rho}\cdot\widetilde{Z''}) + \nabla\cdot(\bar{\rho}\widetilde{\mathbf{u}}\cdot\widetilde{Z''}) = \nabla\cdot\left[\left(\bar{\alpha}+\frac{\bar{\rho}\nu_t}{S\,c_t}\right)\nabla\widetilde{Z''}\right] + C_g\bar{\rho}\nu_t|\nabla\tilde{z}|^2 - C_d\bar{\rho}\frac{\widetilde{\epsilon}}{\widetilde{k}}\cdot\widetilde{Z''} \tag{9}$$

being $\bar{\rho}$ the Reynolds averaged density coming from the tabulated flamelets, ν_t the turbulent viscosity calculated from the standard $k-\epsilon$ turbulence closure model,

$$\nu_t = C_\mu\frac{\widetilde{k}^2}{\widetilde{\epsilon}} \tag{10}$$

DOI: 10.13009/EUCASS2019-353

Pr_t and Sc_t the Prandtl and Schmidt turbulent numbers, C_g, C_d and C_μ model constants equal to 2.86, 2.00 and 0.09 respectively. The pressure-velocity coupling is handled with the PIMPLE operator splitting algorithm.[3] The assessment of the proposed methodology consist in performing first 2D axial-symmetric simulations of a non-adiabatic GOx/GCH4 single-injector combustor developed at TUM, and then 3D simulations of an additional multi-element combustor. Simulation results are compared with experimental data, generally given in terms of wall heat flux and centerline pressure close to the chamber wall.[14,19] For the single injector the former were experientally obtained both via the temperature time derivative in the solid walls (Experiment 1) and cumulative heat flux considerations (Experiment 2). The computational domains are discretized with the finite volume method in a block-structured grid, second and first order accurate in space and time, respectively. The chamber nozzle is not considered since we use a low-Mach numerical framework (for more details about the numerical framework refer to[7]). A grid convergence study has been led for each case. In the following sections it is first presented the 2D campaign on the single injector. This consists of wall resolved simulations as well as with wall functions. For the former a low Reynolds version of the $k-\epsilon$ model is used.[4] For the latter, on the other hand, some parameters need to be established, such as a turbulent Prandtl number σ_t which directly enters in the definition of a turbulent thermal diffusivity at wall and so in the evaluation of the wall heat flux

$$\bar{\alpha}_t^{wall} = \bar{\rho}\frac{\nu_t}{\sigma_t} \tag{11}$$

In eq. (11), σ_t is the aforementioned parameter which we keep separate from the Pr_t entering in the diffusion term of the enthalpy transport equation (8). In the following a methodology to select this parameter based on the results obtained from the wall-resolved simulation will be presented. The settings obtained from the 2D campaign for the wall function simulations are then extended to the 3D case on the multi-element chamber.

3.1 Wall boundary conditions

When dealing with non-adiabatic simulations, a wall temperature profile T_w or a heat flux $\dot{q}_w$ are generally imposed. In the following we will refer to the former situation. Therefore, for a prescribed T_w or, equivalently, an enthalpy h_w, the ensuing $\dot{q}_w$ is calculated as

$$\dot{q}_w = \bar{\alpha}_{eff}\nabla\widetilde{h}|_n \tag{12}$$

being $\bar{\alpha}_{eff}$ an effective thermal diffusivity defined as

$$\bar{\alpha}_{eff} = \bar{\alpha}(\widetilde{Z}_w, \phi_w) + \bar{\alpha}_t^{wall} \tag{13}$$

in which α is a thermal laminar diffusivity (kg/ms) taken from the flamelet libraries for a given enthalpy defect and a mixture fraction value at wall, while $\bar{\alpha}_t^{wall}$ is the turbulent contribution previously defined in eq. (11) coming from the wall functions. Equation (12) is therefore valid both for wall functions and wall resolved simulations. We note from eqs. (12)-(13), the evaluation of the wall heat flux requires the enthalpy value at the wall $\widetilde{h}_w$ for the determination of the gradient, and the value of the defect ϕ_w to select the flamelet from which extract the transport properties at the given mixture fraction value Z_w. The former in particular is reconstructed from eq. (4) once ϕ_w is known, as

$$\widetilde{h}_w = h_{ad}(\widetilde{Z}_w) - \phi_w \cdot f(\widetilde{Z}_w, Z_{st}) \tag{14}$$

The value $\widetilde{h}_w$ is then used to calculate the surface-normal gradient, which in discretized form and referring to a single computational cell is

$$\nabla\widetilde{h}|_n = \frac{\widetilde{h}_w - \widetilde{h}_P}{|\Delta|} \cdot \frac{S_f}{|S_f|} \tag{15}$$

being S_f the cell-face surface, Δ the cell-to-face distance and $\widetilde{h}_P$ the cell-centre value.

4. Results

4.1 2D Wall resolved simulations

For the wall resolved campaign, a final mesh of about 96000 cells have been selected after a grid convergence analysis. An equally spaced discretization is adopted across the domain, except for the near wall regions, where a radial grading is imposed to obtain a width of $0.5\mu m$ for the last cell at the chamber wall. The dimension of an internal field cell is

DOI: 10.13009/EUCASS2019-353

of about 0.14 mm. A comparison between the two flamelet models previously described is first carried out. Following the work done in,[1] a reference Pr_t of 0.895 and a Sc_t of 0.85 are chosen for all the wall resolved simulations. Results are reported in Fig. 6 in terms of wall heat flux.

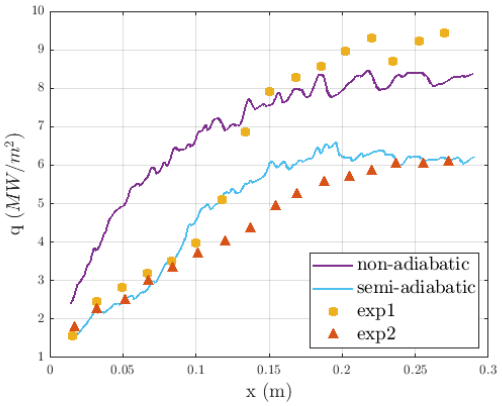

Figure 6: Wall heat flux obtained with the frozen and the non-adiabatic approach compared with experimental data for the wall resolved simulation of the single-injector axial-symmetric chamber.

As observable the non-adiabatic model tends to overestimate the heat flux values, especially in the first half of the chamber, where the difference with the experimental data reach a maximum of approximately 50%. This may be due to the excessive heat released by CO recombination in CO_2 at the wall. This is further investigated by sampling the radial profile of such species and the resulting temperature field across the boundary layer to a section located at 0.1 m. As can be observed from Fig. 7 the flow reaches the wall with a temperature of about 900 K for the non-adiabatic case and almost 550 K for the semi-adiabatic one; this difference directly correlates with the recombination of CO (to CO_2) in the non-adiabatic case, which passes from mass fraction values of 0.4 in the internal field to trace amounts at the wall, thus explaining the differences in the wall heat flux estimation. Further observing Fig. 6, the frozen flamelets, on the other hand, accurately reproduce experimental data until 0.08 m where they seem to follow the second set of experimental values for a short distance, to finally establish on the first again from almost 0.24 m to the end of the simulated geometry. The present analysis of the wall-resolved simulations, thus, seems to suggest not to consider wall recombinations for the operative conditions and the chosen simulation settings.

4.2 2D Wall modeled simulations

A 2D simulation of the same chamber is then performed on a different grid employing wall functions. Following the previous results, the frozen set of flamelets is used together with a turbulent Prandtl and a turbulent Schmidt number inherited from the wall resolved simulation, i.e $Pr_t = 0.895$ and $Sc_t = 0.85$. The purpose is to reproduce the results

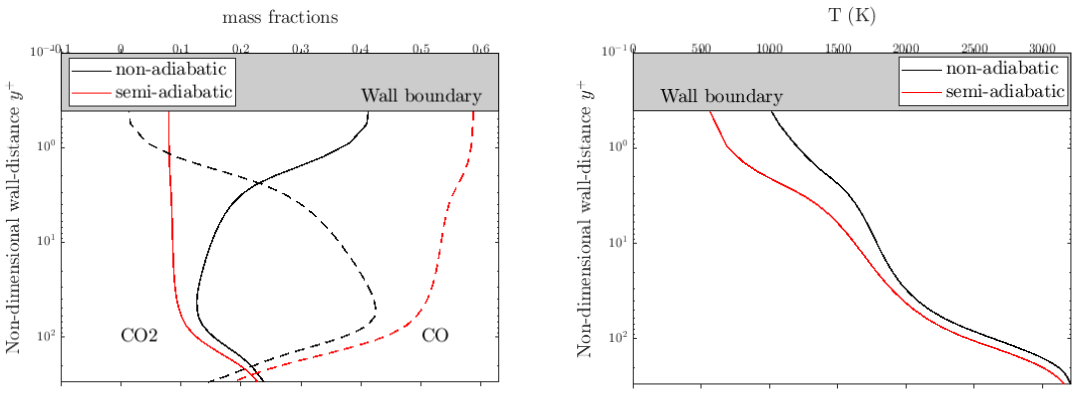

Figure 7: Radial CO and CO_2 mass fractions profiles (left) and temperature (right) across the boundary layer as function of y^+, for the semi-adiabatic and the non-adiabatic wall resolved simulations.

DOI: 10.13009/EUCASS2019-353

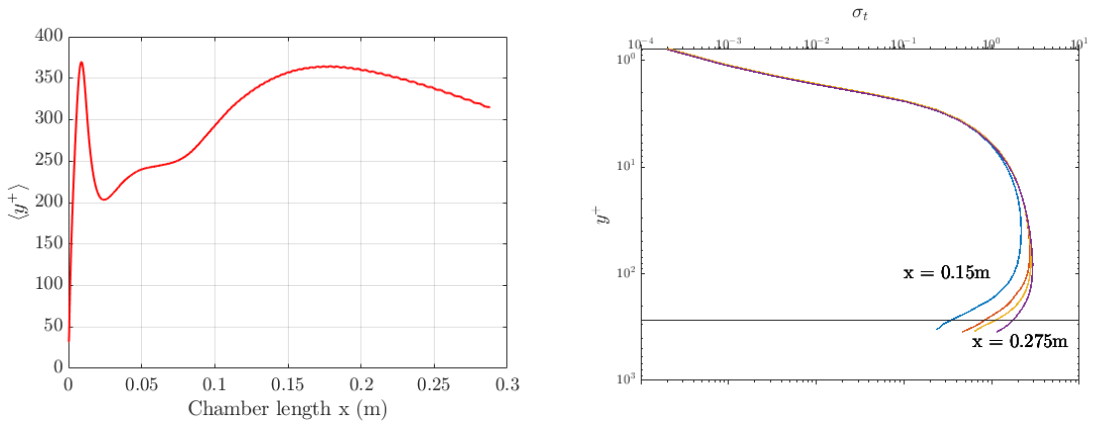

Figure 8: Left: y^+ values at wall for the axial symmetric simulation employing wall functions. Right: radial profiles of the wall function parameter σ_t as a function of the non-dimensional distance from the wall, for different sections along the chamber.

previously obtained having introduced the wall function model. The use of wall functions, however, mitigates the differences between the non-adiabatic and the frozen models, the last computational node at wall generally lying at a non-dimensional wall distance y^+ ranging between 30 and 300 (see Fig. 7). The introduction of a turbulent quantity σ_t, different from the one controlling the diffusion of enthalpy Pr_t, is therefore necessary to coherently model near wall phenomena which are in general neglected by wall functions. In the following a methodology is proposed for the calibration of this parameter, depending on the y^+ expected from the wall function simulation. From the previous wall resolved results, a wall heat flux $\dot{q}(y^+)$ is defined by progressively reconstructing an enthalpy gradient $\nabla\widetilde{h}|_n(y^+)$ at differents distances Δy from the wall and by considering the laminar diffusivity at wall $\bar{\alpha}$, as

$$\dot{q}(y^+) = \bar{\alpha}\, \nabla\widetilde{h}|_n(y^+) \tag{16}$$

$$\nabla\widetilde{h}|_n(y^+) = \frac{\widetilde{h}_w - \widetilde{h}(y^+)}{\Delta y} \tag{17}$$

in which $\widetilde{h}(y^+)$ is the enthalpy at the considered y^+ distance from the wall. Equations (12)-(13) can be rewritten as

$$\dot{q}_w = (\bar{\alpha} + \bar{\alpha}_t^{wall})\nabla\widetilde{h}|_n(y^+) = \dot{q}(y^+) + \frac{\bar{\rho}(y^+)\nu_t(y^+)}{\sigma_t}\nabla\widetilde{h}(y^+). \tag{18}$$

A turbulent Prandtl number σ_t is then defined inverting eq. (18) and imposing $\dot{q}_w$ equal to the wall heat flux $\dot{q}^{WR}$ ensuing from the wall resolved simulation (Fig. 6), ending up with

$$\sigma_t = \frac{\bar{\rho}(y^+)\nu_t(y^+)}{\dot{q}^{WR} - \dot{q}(y^+)}\, \nabla\widetilde{h}|_n(y^+) \tag{19}$$

In this way we obtain σ_t as a function of y^+, i.e a table which can be consulted in order to consistently tune the wall function parameter, according to the estimated y^+. For the present simulation we have a mesh characterized by an integral y^+ value of about 270 along the chamber wall; from Fig. 8 it is shown that, for that value, σ_t varies between 0.1 and 1.2 along the chamber. Since we are considering an integral value of y^+ which is mainly attained in the second half of the chamber, as shown in Fig. 8, the selected value for σ_t is 0.95.
The results of this tuning technique are reported in Fig 9 and show an overall good agreement with experimental data, except for the first part where the latter are underestimated. The reason can be traced back to the previous assumptions limiting the choice of the σ_t value, whose selection was based on a mean y^+ value.

4.3 3D simulations

The settings previously obtained for the wall function simulation on the single injector are then extended to the seven-element GOx/GCH4 multi-injector combustor,[14] employing for the two chambers the same sets of flamelets. The new non-adiabatic model is again tested against experiments and results obtained with the semi-adiabatic approach. A 60-degree computational domain was chosen, taking advantage of the chamber symmetry, resulting in a computational grid

DOI: 10.13009/EUCASS2019-353

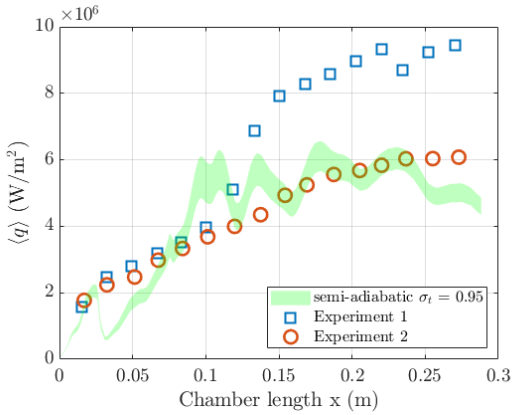

Figure 9: Comparison between experiment (symbols) and the axial symmetric simulations (continuos line shaded by variance) for the frozen version of the new non-adiabatic model in terms of wall heat flux at the chamber wall.

of 182300 cells. Wall functions for the turbulent quantities $\widetilde{k}$, $\widetilde{\epsilon}$, ν_t and α_t are employed to save computational resources according to the formulation proposed in.[5]Non-adiabatic boundary conditions are enforced on the upper chamber wall, where a temperature profile obtained by experiments is prescribed; adiabatic conditions are enforced for the plate and the post-tip wall. A view of the chamber and of a sliced temperature field is given in Fig. 10 while a summary of the obtained wall heat fluxes with the three models and the wall pressure profile is given in Fig. 11.

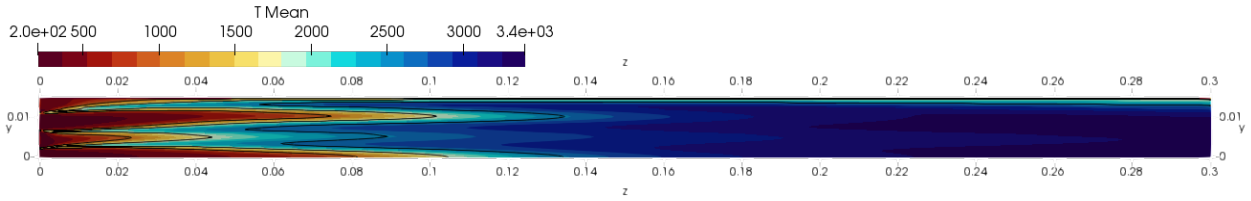

Figure 10: Time averaged temperature field in a longitudinal slice of the seven element combustor obtained using the non-adiabatic approach.

In the first chamber segment all the models tend to underestimate experimental values while in the second one the differences with the non-adiabatic model are almost neglegible. Indeed, differently from the 2D case, here the non-adiabatic model seem to perform better than the frozen model, especially in the first two chamber segments. In the third segment on the other hand, the frozen and the non-adiabatic models are almost equally spaced, respectively below and above experiments.

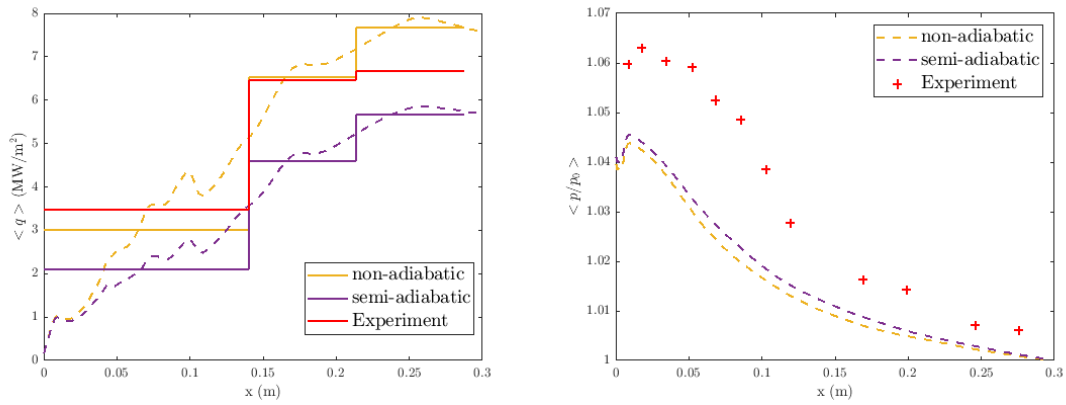

Figure 11: Comparison between 3D numerical and experimental wall heat flux (left) and pressure drop (right) for the seven element chamber, obtained with the new non-adiabatic model and the frozen approach

DOI: 10.13009/EUCASS2019-353

5. Conclusions

In this work we have developed and validated a modeling strategy for the evaluation of wall heat fluxes within the operative conditions of liquid rocket engines combustion chambers. Such a methodology is based on the non-adiabatic flamelet concept and can be used in both wall resolved and wall modeled simulations. A well known single element combustion chamber has been simulated in a wall resolved fashion to firstly assess the best tabulation technique fitting experimental data. For the chosen numerical settings, results suggested to select the frozen or semi-adiabatic approach in the flamelets generation. An other simulation of the same combustor, employing the chosen set of flamelets and a wall modeled boundary layer, has been then carried out with a properly calibrated turbulent Prandtl number at wall. The ensuing wall heat flux has been shown to correctly reproduce the results obtained on the wall resolved simulation, and so the experiment, providing model validation. Finally, a 3D simulation of a multi-element chamber has been carried out to further assess model performances, showing a good agreement with experimental results.

Acknowledgment

This work is carried out with the support of the Italian Ministry of University and Research (MIUR).

References

[1] A Chemnitz, Thomas Sattelmayer, Christof Roth, Oskar Haidn, Yu Daimon, R Keller, P Gerlinger, Julian Zips, and Michael Pfitzner. Numerical investigation of reacting flow in a methane rocket combustor: Turbulence modeling. *Journal of Propulsion and Power*, pages 1–14, 12 2017.

[2] Alberto Cuoci, Alessio Frassoldati, T Faravelli, and Eliseo Ranzi. Opensmoke++: An object-oriented framework for the numerical modeling of reactive systems with detailed kinetic mechanisms. *Computer Physics Communications*, 192:237–264, 2015.

[3] J. H. Ferziger and M. Peric. *Computational methods for fluid dynamics*. Springer Science Business Media, 2012.

[4] Launder B.E.. Jones, W.P. The prediction of laminarization with a two-equation model of turbulence. *International Journal of Heat and Mass Transfer*, 15:301–314, 1972.

[5] Georgi Kalitzin, Gorazd Medic, Gianluca Iaccarino, and Paul Durbin. Near-wall behavior of ransturbulence models and implications for wall functions. *Computational physics*, 204(205):23–48, 2004.

[6] Seong-Ku Kim, Miok Joh, Hwan Seok Choi, and Tae Seon Park. Multidisciplinary simulation of a regeneratively cooled thrust chamber of liquid rocket engine: Turbulent combustion and nozzle flow. *International Journal of Heat and Mass Transfer*, 70:1066–1077, 2014.

[7] P. E. Lapenna, R. Amaduzzi, D. Durigon, G. Indelicato, F. Nasuti, and F. Creta. Simulation of a single-element gch4/gox rocket combustor using a non-adiabatic flamelet method. page 4872, 2018.

[8] P. E. Lapenna and F. Creta. Mixing under transcritical conditions: an a-priori study using direct numerical simulation. *The Journal of Supercritical Fluids*, in press, 2017.

[9] P. E. Lapenna, G. Indelicato, R. Lamioni, and F. Creta. Modeling the equations of state using a flamelet approach in lre-like conditions. *ACTA Astronautica*, 2018.

[10] P.E. Lapenna, G. Indelicato, R. Amaduzzi, D. Durigon, and F. Creta. Consistent flamelet-based turbulent combustion modeling for liquid rocket engines. *Joint meeting the german and italian sections of the combustion institute*, 2018.

[11] Peter C Ma, Hao Wu, Matthias Ihme, Hickey, and Jean-Pierre. Nonadiabatic flamelet formulation for predicting wall heat transfer in rocket engines. *AIAA Journal*, 56(6):2336–2349, 2018.

[12] B. Marracino and D. Lentini. Radiation modelling in non-luminous nonpremixed turbulent flames. *Combustion Science and Technology*, 128:23–48, 1997.

[13] J. C. Oefelein. Mixing and combustion of cryogenic oxygen-hydrogen shear-coaxial jet flames at supercritical pressure. *Combust. Sci. Technol.*, 178:229–252, 2006.

DOI: 10.13009/EUCASS2019-353

[14] C. Maria Palma, S. Silvestri, G. Schlieben, C. Kirchberger, O. Haidn, and O. Knab. Injector characterization for a gaseous oxygen-methane single element combustion chamber. *Progress in Propulsion Physics*, 8:145–164, 2016.

[15] Nikolaos Perakis, Christof Roth, and Oskar Haidn. Development of a non-adiabatic flamelet model for reacting flows with heat loss. 05 2018.

[16] N. Peters. *Turbulent Combustion*. Cambridge University Press, UK, Cambridge, UK, 2000.

[17] Thierry Poinsot and Denis Veynante. *Theoretical and numerical combustion*. RT Edwards Inc., Philadelphia, PA, 2005.

[18] P.Wollny, B.Rogg, and A. Kempf. Modelling heat loss effects in high temperature oxy-fuel flames with an efficient and robust non-premixed flamelet approach. *Fuel*, 216:44–52, 2018.

[19] S. Silvestri, M. P. Celano, G. Schlieben, and O. Haidn. Characterization of a multi-injector gox-gch4 combustion chamber. *52nd AIAA/SAE/ASEE Paper*, 2016.

[20] Golden D. M. Frenklach M. Moriarty N. W. Eiteneer B. Goldenberg M. Bowman C. Hanson R. Song S. Gardiner Jr W. et al. Smith, G. P. Gri-mech 3.0, 2000. URL http://www. me. berkeley. edu/gri. mech.

[21] Paul Tucker, Suresh Menon, Charles Merkle, Joseph Oefelein, and Vigor Yang. Validation of high-fidelity cfd simulations for rocket injector design. page 5226, 2008.

[22] Yi Wang and Arnaud Trouvé. Direct numerical simulation of nonpremixed flame–wall interactions. *Combustion and flame*, 144(3):461–475, 2006.

[23] Julian Zips, Hagen Müller, and Michael Pfitzner. Non-adiabatic tabulation methods to predict wall-heat loads in rocket combustion. page 1469, 2017.